Physics Letters A 372 (2008) 4344–4349

Contents lists available at ScienceDirect

Physics Letters A

www.elsevier.com/locate/pla

Tachyonic γ-ray spectra of active galactic nuclei: Evidence for intrinsic spectral curvature

Roman Tomaschitz *

Department of Physics, Hiroshima University, 1-3-1 Kagami-yama, Higashi-Hiroshima 739-8526, Japan

ARTICLE INFO

Article history:
Received 18 February 2008
Received in revised form 15 April 2008
Accepted 15 April 2008
Available online 18 April 2008
Communicated by V.M. Agranovich

PACS:
03.50.Kk
05.30.Fk
52.27.Ny
95.30.Gv

Keywords:
Superluminal radiation
Tachyonic cascade spectra
Ultra-relativistic electron plasma
TeV blazars
Spectral averaging
Proca equation with negative mass-square

ABSTRACT

Tachyonic spectral densities of ultra-relativistic electron populations are fitted to the γ-ray spectra of two TeV blazars, the BL Lacertae objects 1ES 0229+200 and 1ES 0347-121. The spectral maps are compared to Galactic TeV sources, the γ-ray binary LS 5039 and the supernova remnant W28. In contrast to TeV photons, the extragalactic tachyon flux is not attenuated by interaction with the cosmic background light; there is no absorption of tachyonic γ-rays via pair creation, as tachyons do not interact with infrared background photons. The curvature of the observed γ-ray spectra is intrinsic, caused by the Boltzmann factor of the electron densities, and reproduced by a tachyonic cascade fit. In particular, the curvature in the spectral map of the Galactic microquasar is more pronounced than of the two extragalactic γ-ray sources. Estimates of the thermodynamic parameters of the thermal or, in the case of supernova remnant W28, shock-heated nonthermal electron plasma generating the tachyon flux are obtained from the spectral fits.

1. Introduction

The goal is to point out evidence for superluminal γ-rays from two active galactic nuclei, the BL Lacertae objects 1ES 0229+200, cf. Refs. [1–4], and 1ES 0347-121, cf. Refs. [5–7]. Spectral maps of these TeV blazars have recently been obtained by means of ground-based imaging air Cherenkov detectors [4,7]. Here, a tachyonic cascade fit is performed to the γ-ray spectrum of these blazars. In contrast to electromagnetic γ-rays, tachyons cannot interact with infrared background photons, so that there is no attenuation of the extragalactic tachyon flux by electron–positron pair production. The observed spectrum is already the intrinsic one without any need of absorption correction as required in electromagnetic spectral fits [8,9]. The spectral curvature is generated by the Boltzmann factor of the thermal electron plasma in the galactic nuclei.

Tachyonic cascade spectra are obtained by averaging the superluminal spectral densities of individual electrons with ultra-relativistic Fermi distributions. We use the averaged radiation densities to perform spectral fits to the γ-ray spectra of the mentioned BL Lacertae objects as well as the microquasar LS 5039 and the supernova remnant W28. Tachyonic cascade spectra generated by thermal electron populations in the active galactic nuclei (AGNs) provide excellent fits to the observed γ-ray flux. The temperature, source count, and internal energy of the ultra-relativistic electron plasma are obtained from the spectral fits. The spectral map of the Galactic microquasar is no less curved than the cascades in the AGN spectra. Moreover, the spectral curvature of the AGNs does not increase with increasing redshift, which is further evidence for an unattenuated extragalactic γ-ray flux.

The tachyonic radiation field is a Proca field with negative mass-square,

$$L_{\mathrm{P}} = -\frac{1}{4} F_{\alpha\beta} F^{\alpha\beta} + \frac{1}{2} m_{\mathrm{t}}^2 A_\alpha A^\alpha + A_\mu j^\mu, \tag{1}$$

coupled to an electron current $j^\mu = -q\bar{\psi}\gamma^\mu\psi$, where m_{t} is the mass of the superluminal Proca field A_α, and q the tachyonic charge carried by the subluminal current [10–12]. The mass term in (1) is added with a positive sign, and the sign convention for the metric is diag$(-1,1,1,1)$, so that $m_{\mathrm{t}}^2 > 0$ is the negative mass-square of the radiation field. The sign convention for the field tensor is $F_{\mu\nu} = A_{\nu,\mu} - A_{\mu,\nu}$. The negative mass-square refers to the

---

* Tel.: +81 824 247361; fax: +81 824 240717.
E-mail address: tom@geminga.org.

0375-9601/$ – see front matter © 2008 Elsevier B.V. All rights reserved.
doi:10.1016/j.physleta.2008.04.026

radiation field rather than the current, in contrast to the traditional approach based on superluminal source particles emitting electromagnetic radiation [13,14]. The superluminal radiation field does not carry any kind of charge, tachyonic charge q is a property of subluminal particles, as is electric charge [15]. The field equations derived from (1) read ${F^{\mu\nu}}_{,\nu} - m_t^2 A^\mu = j^\mu$, and can equivalently be written as Proca equation, $(\partial^\nu \partial_\nu + m_t^2)A_\mu = -j_\mu$, subject to the Lorentz condition ${A^\mu}_{,\mu} = 0$, which follows from current conservation ${j^\mu}_{,\mu} = 0$. An estimate of the tachyon–electron mass ratio obtained from hydrogenic Lamb shifts is $m_t/m \approx 1/238$ [16].

In Section 2, we further elaborate on the tachyonic Proca equation by comparing to electromagnetic theory, and assemble the tachyonic spectral averages employed in the fits, which are based on the transversal and longitudinal radiation densities generated by a free electronic spinor current. In Section 3, the spectral fitting is explained, and intrinsic spectral curvature is argued by comparing the cascade spectra of the above-mentioned Galactic and extragalactic TeV sources. The conclusions are summarized in Section 4.

2. Spectral maps in the γ-ray bands: Origin and structure of tachyonic cascade spectra

The Lagrangian (1) resembles its electrodynamic counterpart, but the negative mass-square of the Proca field causes striking differences. Apart from the superluminal speed of the tachyonic quanta, the radiation is partially longitudinally polarized [12], the gauge freedom is broken, and freely propagating charges can radiate superluminal quanta. The analogy to Maxwell's theory becomes even more transparent in 3D. The tachyonic $\mathbf{E}$ and $\mathbf{B}$ fields are related to the vector potential $A_\alpha = (A_0, \mathbf{A})$ by $\mathbf{E} = \nabla A_0 - \partial \mathbf{A}/\partial t$ and $\mathbf{B} = \operatorname{rot} \mathbf{A}$, and the field equations decompose into

$$\operatorname{div} \mathbf{B} = 0, \qquad \operatorname{rot} \mathbf{E} + \partial \mathbf{B}/\partial t = 0,$$
$$\operatorname{div} \mathbf{E} = \rho - m_t^2 A_0, \qquad \operatorname{rot} \mathbf{B} - \partial \mathbf{E}/\partial t = \mathbf{j} + m_t^2 \mathbf{A}, \tag{2}$$

where we identified $j^\mu = (\rho, \mathbf{j})$. The vector potential is completely determined by the current and the field strengths; there is no gauge freedom owing to the tachyon mass. Another major difference to electromagnetic theory is the emergence of longitudinal wave propagation. To see this, we consider monochromatic waves, $\mathbf{A}(\mathbf{x}, t) = \hat{\mathbf{A}}(\mathbf{k}) \mathrm{e}^{\mathrm{i}(\mathbf{kx} - \omega t)} + \text{c.c.}$, and analogously for the scalar potential and the field strengths, with amplitudes $\hat{A}_0(\mathbf{k}), \hat{\mathbf{E}}(\mathbf{k})$, and $\hat{\mathbf{B}}(\mathbf{k})$, respectively. We write $\mathbf{k} = k(\omega)\mathbf{k}_0$, with a unit wave vector $\mathbf{k}_0$. On substituting this ansatz into the free field equations (2), we find the dispersion relation $k = \sqrt{\omega^2 + m_t^2}$. The transversality condition on the vector potential is $\hat{\mathbf{A}}\mathbf{k}_0 = 0$, so that the remaining transversal amplitudes are $\hat{A}_0 = 0, \hat{\mathbf{E}} = \mathrm{i}\omega \hat{\mathbf{A}}$, and $\hat{\mathbf{B}} = \mathrm{i}k(\omega)\mathbf{k}_0 \times \hat{\mathbf{A}}$. If the product $\hat{\mathbf{A}}\mathbf{k}_0$ does not vanish, the modes must be longitudinal, satisfying $\hat{\mathbf{A}} = (\hat{\mathbf{A}}\mathbf{k}_0)\mathbf{k}_0$. In this case, $\hat{A}_0 = -(k/\omega)\mathbf{k}_0 \hat{\mathbf{A}}, \hat{\mathbf{E}} = -\mathrm{i}(m_t^2/\omega)\hat{\mathbf{A}}$, and $\hat{\mathbf{B}} = 0$, so that a longitudinal plane wave has no magnetic component.

The spectral fits in Section 3 are based on the quantized tachyonic radiation densities

$$p^{\mathrm{T,L}}(\omega, \gamma) = \frac{\alpha_q m_t^2 \omega}{\omega^2 + m_t^2} \left[\gamma^2 - \frac{m_t}{m} \frac{\omega}{m_t} \gamma - \frac{1}{4} \frac{m_t^2}{m^2} - \left(1 + \frac{\omega^2}{m_t^2}\right) \Delta^{\mathrm{T,L}} \right] \frac{1}{\gamma \sqrt{\gamma^2 - 1}}, \tag{3}$$

generated by the spinor current $j^\mu = -q\bar{\psi}\gamma^\mu\psi$ of a uniformly moving electron [11]. The superscripts T and L refer to the transversal/longitudinal polarization components defined by $\Delta^{\mathrm{T}} = 1 - m_t^2/(2m^2)$ and $\Delta^{\mathrm{L}} = 0$. γ is the electronic Lorentz factor, α_q the tachyonic fine structure constant, and m_t the tachyon mass. In the γ-ray broadband fit of supernova remnant W28, the radiation frequencies ω stretch over five decades, cf. Section 3. The units $\hbar = c = 1$ can easily be restored. We use the Heaviside–Lorentz system, so that $\alpha_q = q^2/(4\pi\hbar c) \approx 1.0 \times 10^{-13}$ and $m_t \approx 2.15\ \mathrm{keV}/c^2$; the tachyon–electron mass ratio is $m_t/m \approx 1/238$. These estimates are obtained from Lamb shifts of hydrogenic ions [16]. A spectral cutoff occurs at

$$\omega_{\max}(\gamma) = m_t \left(\mu_t \sqrt{\gamma^2 - 1} - \frac{1}{2} \frac{m_t}{m} \gamma \right), \qquad \mu_t := \sqrt{1 + \frac{1}{4} \frac{m_t^2}{m^2}}. \tag{4}$$

Only frequencies in the range $0 \leqslant \omega \leqslant \omega_{\max}(\gamma)$ can be radiated by a uniformly moving electron, the tachyonic spectral densities $p^{\mathrm{T,L}}(\omega, \gamma)$ being cut off at the break frequency $\omega_{\max}$. A positive $\omega_{\max}(\gamma)$ requires Lorentz factors exceeding the threshold μ_t in (4), since $\omega_{\max}(\mu_t) = 0$. The lower threshold on the speed of the electron for radiation to occur is thus $\upsilon_{\min} = m_t/(2m\mu_t)$. The tachyon–electron mass ratio gives $\upsilon_{\min}/c \approx 2.1 \times 10^{-3}$, which is roughly the speed of the Galaxy in the microwave background [17].

The radiation densities (3) refer to a single spinning charge with Lorentz factor γ; we average them with a Fermi power-law distribution [18,19],

$$\mathrm{d}\rho_{\mathrm{F}}(\gamma) = \frac{m^3 V}{\pi^2} \frac{\sqrt{\gamma^2 - 1}\gamma \, \mathrm{d}\gamma}{1 + \gamma^\delta \mathrm{e}^{\beta\gamma + \hat{\alpha}}}. \tag{5}$$

The particle number is found as $n_1 = \int_{\gamma_1}^\infty \mathrm{d}\rho_{\mathrm{F}}(\gamma)$, where γ_1 is the lower edge of Lorentz factors in the source population. m is the electron mass, and the exponential cutoff is related to the electron temperature by $\beta = m/(kT)$. The power-law exponent δ ranges in a narrow interval in astrophysical spectral averages [20–28], which are usually done in the classical limit (13) with $0 \leqslant \delta \leqslant 4$. Otherwise, there are no conceptual constraints on the power-law index of these stationary non-equilibrium distributions. Thermal equilibrium is recovered with $\delta = 0$ and $\gamma_1 = 1$; the spectral fits of the blazars and the microquasar in Figs. 1–3 are performed with equilibrium distributions. The shocked electron plasma of supernova remnant W28 requires $\delta \approx 3.6$ to fit the steep power-law slope in Fig. 4. The exponent $\hat{\alpha}$ in (5) defines the fugacity $\mathrm{e}^{-\hat{\alpha}}$; we use a hat to distinguish $\hat{\alpha}$ from the electron index customarily defined as $\alpha = \delta - 2$, cf. (13). The fugacity is related to the chemical potential μ by $\hat{\alpha} = -\beta\mu/m$.

The spectral average of the radiation densities (3) is carried out as

$$\langle p^{\mathrm{T,L}}(\omega) \rangle_{\mathrm{F}} := \int_{\gamma_1}^{\infty} p^{\mathrm{T,L}}(\omega, \gamma) \theta\big(\omega_{\max}(\gamma) - \omega\big) \, \mathrm{d}\rho_{\mathrm{F}}(\gamma), \tag{6}$$

where θ is the Heaviside step function. The spectral range of densities (3) is bounded by $\omega_{\max}$ in (4), so that the solution of $\omega = \omega_{\max}(\hat{\gamma})$ defines the minimal electronic Lorentz factor for radiation at this frequency [29],

$$\hat{\gamma}(\omega) = \mu_t \sqrt{1 + \frac{\omega^2}{m_t^2}} + \frac{1}{2} \frac{m_t}{m} \frac{\omega}{m_t}. \tag{7}$$

The average (6) can be reduced to the fermionic spectral functions

$$F^{\mathrm{T,L}}(\omega, \gamma_1) := \int_{\gamma_1}^{\infty} p^{\mathrm{T,L}}(\omega, \gamma) \, \mathrm{d}\rho_{\mathrm{F}}(\gamma), \tag{8}$$

with lower integration boundary $\gamma_1 \geqslant \mu_t$, cf. after (4). This threshold Lorentz factor γ_1 defines the break frequency,

$$\omega_1 := \omega_{\max}(\gamma_1) = m_t \left(\mu_t \sqrt{\gamma_1^2 - 1} - \frac{1}{2} \frac{m_t}{m} \gamma_1 \right), \tag{9}$$

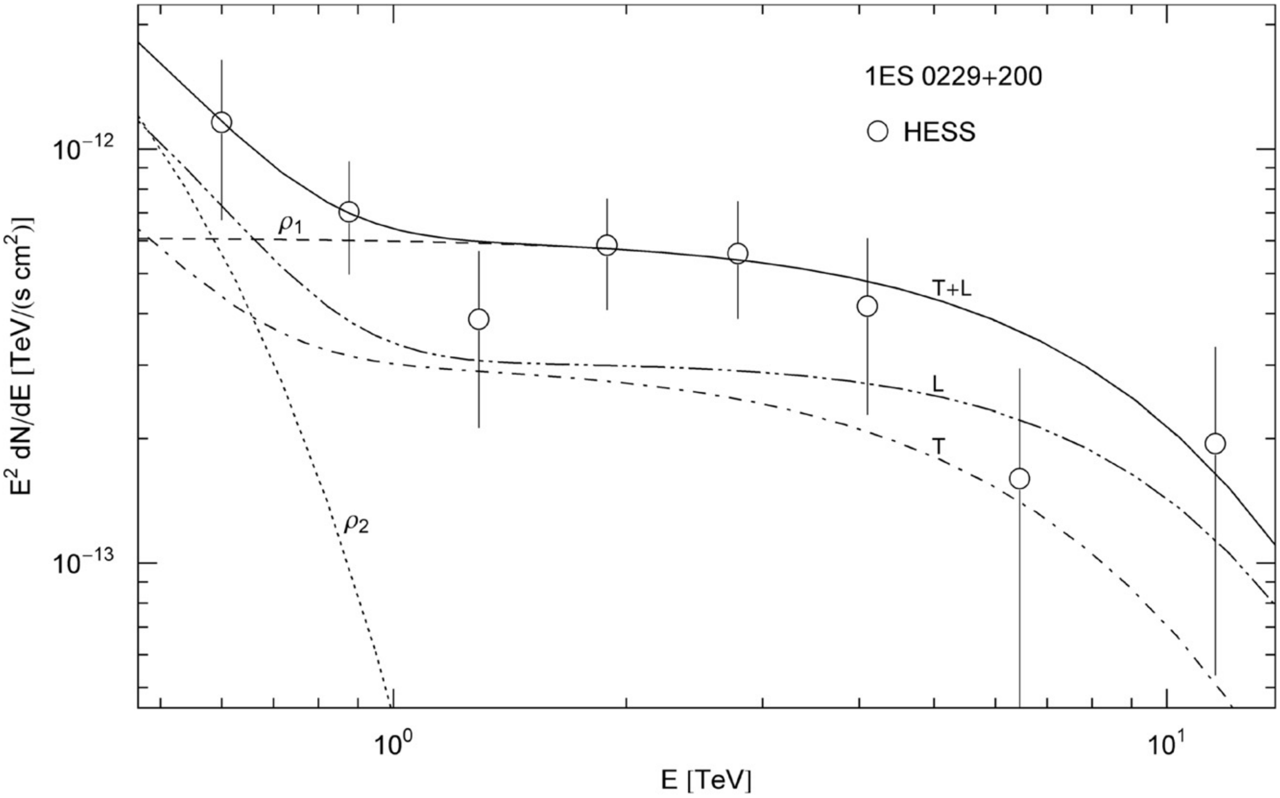

Fig. 1. Spectral map of the BL Lac 1ES 0229+200. HESS data points from [4]. The solid line T + L depicts the unpolarized differential tachyon flux $\mathrm{d}N^{\mathrm{T+L}}/\mathrm{d}E$, obtained by adding the flux densities $\rho_{1,2}$ of two electron populations, cf. (16) and Table 1. The transversal (T, dot-dashed) and longitudinal (L, double-dot-dashed) flux densities add up to the total unpolarized flux T + L. The exponential decay of the cascades $\rho_{1,2}$ sets in at about $E_{\mathrm{cut}} \approx (m_t/m)kT$, implying cutoffs at 3.6 TeV for the ρ_1 cascade and 120 GeV for ρ_2.

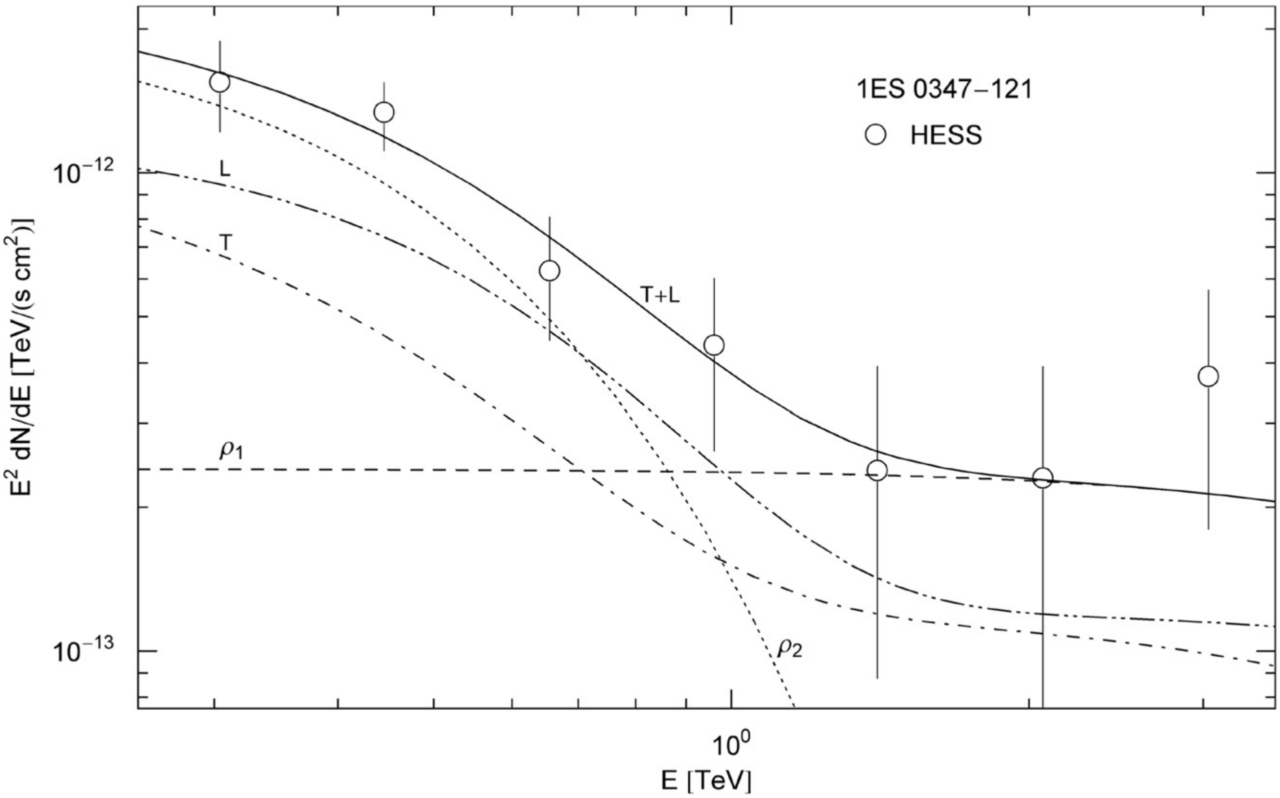

Fig. 2. Spectral map of the BL Lac 1ES 0347-121. HESS points from [7]. The unpolarized spectral fit T + L is based on the electron distributions recorded in Table 1, the polarized flux components are labeled T and L. The ρ_1 cascade is cut at $E_{\mathrm{cut}} \approx 4.0$ TeV, and ρ_2 at 190 GeV. The curvature in the spectral slope of 1ES 0347-121 at $z \approx 0.188$ is less pronounced than of 1ES 0229+200 at $z \approx 0.140$, suggesting that the shape of the rescaled flux density $E^2\,\mathrm{d}N^{\mathrm{T+L}}/\mathrm{d}E$ is intrinsic rather than generated by intergalactic absorption.

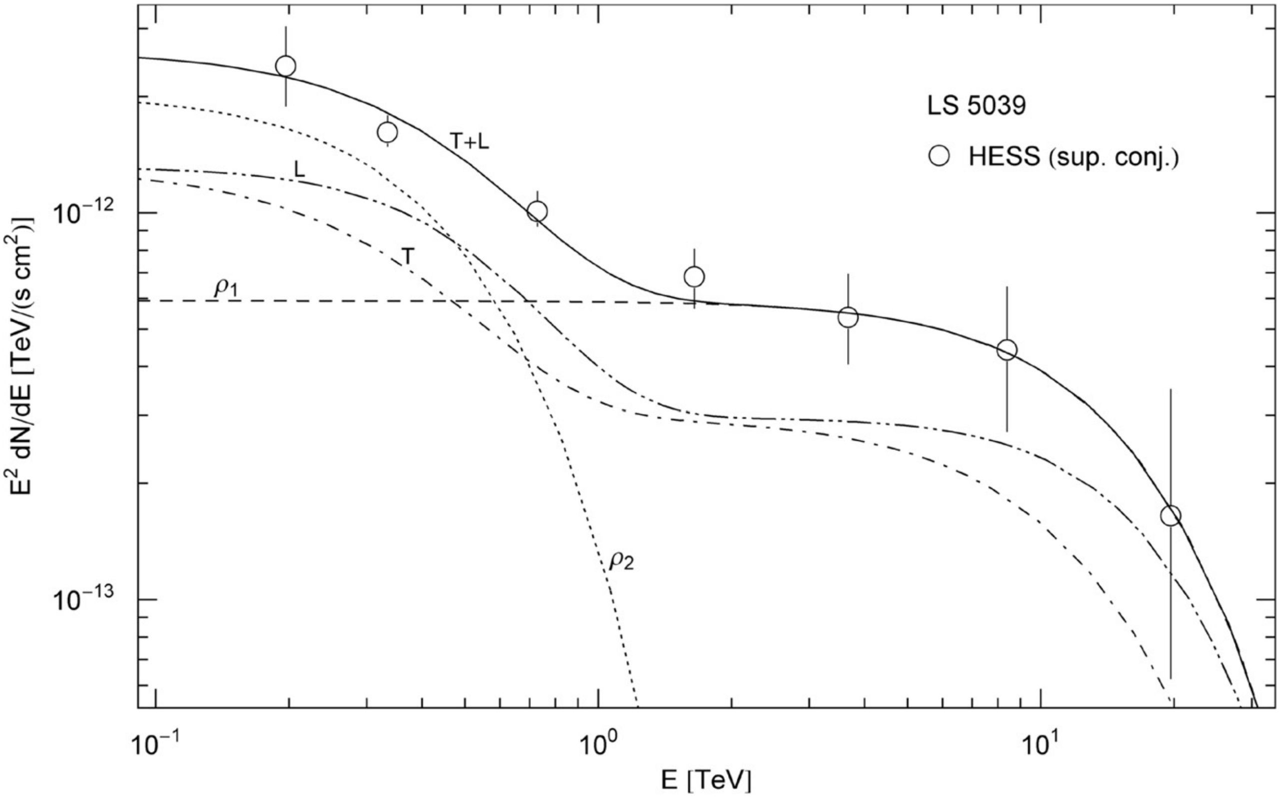

Fig. 3. Spectral map of the γ-ray binary LS 5039 close to periastron. HESS data points at the superior conjunction [32]. Notation as in Fig. 1. The cascade ρ_1 is exponentially cut at $E_{\mathrm{cut}} \approx 6.3$ TeV, and ρ_2 at 190 GeV, cf. Table 1. The spectral map of this microquasar at a distance of 2.5 kpc is more strongly curved than of the AGNs in Figs. 1 and 2, indicating that the curvature of the AGN spectra is intrinsic as well, generated by the Boltzmann factor of the thermal electron populations, cf. caption to Fig. 2.

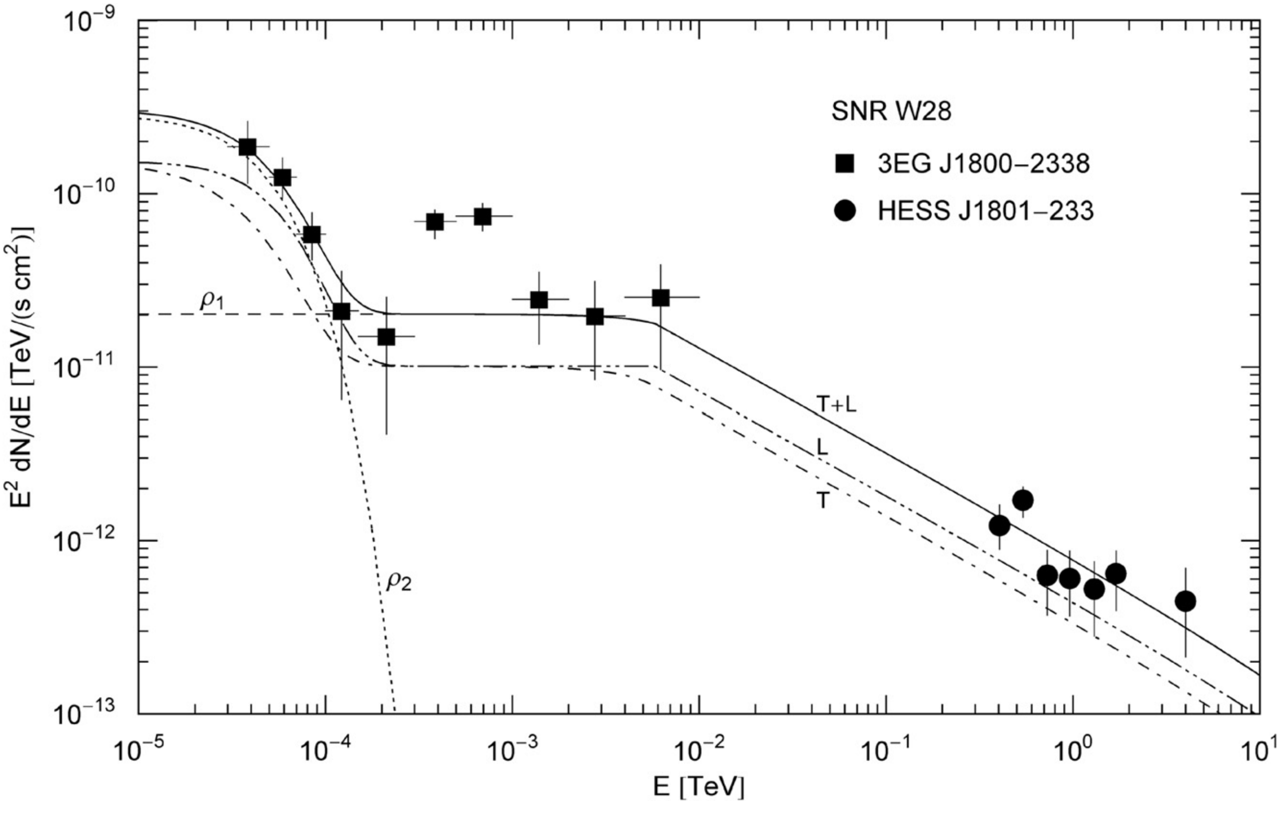

Fig. 4. γ-Ray broadband of the TeV source HESS J1801-233 and the associated EGRET source 3EG J1800-2338 at the northeast boundary of supernova remnant W28. Data points from [35], also see [36,37]. Notation as in Fig. 1. The nonthermal cascade ρ_1 admits a power-law slope $\propto E^{1-\alpha}$, $\alpha \approx 1.6$, adjacent to the MeV–GeV plateau typical for tachyonic cascade spectra [11,12]. A spectral break at $m_t\gamma_1 \approx 5.8$ GeV is visible as edge in the longitudinal component. The curvature of the thermal cascade ρ_2 in the MeV range is due to the exponential cutoff at $(m_t/m)kT \approx 20$ MeV, cf. Table 1.

Table 1

Electronic source distributions ρ_i generating the tachyonic cascade spectra of the active galactic nuclei in Figs. 1 and 2, the microquasar LS 5039 in Fig. 3, and the supernova remnant W28 in Fig. 4. Each ρ_i stands for a thermal Maxwell–Boltzmann density $\mathrm{d}\rho_{\alpha=-2,\beta}(\gamma)$ with $\gamma_1 = 1$, apart from the ρ_1 distribution of SNR W28, which is a power-law density with $\alpha \approx 1.6$ and $\gamma_1 \approx 2.7 \times 10^6$, cf. (13) and after (5). β is the cutoff parameter in the Boltzmann factor. $\hat{n}$ determines the amplitude of the tachyon flux generated by the electron density ρ_i, from which the electron count n^{e} is inferred at the indicated distance d, cf. after (17). kT is the temperature and U the internal energy of the electron populations, cf. after (16). The parameters β and $\hat{n}$ are extracted from the least-squares fit T + L in Figs. 1–4

	β	$\hat{n}$	d	n^{e}	kT (TeV)	U (erg)
1ES 0229+200			$z \approx 0.140$			
ρ_1	5.97×10^{-10}	6.6×10^{-5}	620 Mpc	1.4×10^{57}	860	5.8×10^{60}
ρ_2	1.79×10^{-8}	7.5×10^{-4}		1.6×10^{58}	29	2.2×10^{60}
1ES 0347-121			$z \approx 0.188$			
ρ_1	5.38×10^{-10}	2.6×10^{-5}	830 Mpc	1.0×10^{57}	950	4.6×10^{60}
ρ_2	1.13×10^{-8}	2.3×10^{-4}		8.9×10^{57}	45	1.9×10^{60}
LS 5039 (sup. conj.)			2.5 kpc			
ρ_1	3.36×10^{-10}	6.4×10^{-5}		2.3×10^{46}	1500	1.7×10^{50}
ρ_2	1.13×10^{-8}	2.2×10^{-4}		7.9×10^{46}	45	1.7×10^{49}
SNR W28			1.9 kpc			
ρ_1	–	2.2×10^{-3}		4.6×10^{47}	–	–
ρ_2	1.08×10^{-4}	3.1×10^{-2}		6.4×10^{48}	4.7×10^{-3}	1.5×10^{47}

which separates the spectrum into a low- and high-frequency band [30]. By making use of the spectral functions (8), we can write the averaged radiation densities (6) as

$$\left\langle p^{\mathrm{T,L}}(\omega)\right\rangle_{\mathrm{F}} = F^{\mathrm{T,L}}(\omega,\gamma_1)\theta(\omega_1-\omega) + F^{\mathrm{T,L}}\big(\omega,\hat{\gamma}(\omega)\big)\theta(\omega-\omega_1), \tag{10}$$

with $\hat{\gamma}(\omega)$ in (7) and ω_1 in (9), so that $\hat{\gamma}(\omega_1) = \gamma_1$. The superscripts T and L denote the transversal and longitudinal radiation components, cf. (3). The spectral functions $F^{\mathrm{T,L}}(\omega,\gamma_1)$ in (10) are obtained by substituting radiation densities (3) into the integral representation (8),

$$F^{\mathrm{T,L}}(\omega,\gamma_1) = \frac{\alpha_{\mathrm{q}} m_{\mathrm{t}}^2 \omega}{\omega^2+m_{\mathrm{t}}^2}\left[f_3(\gamma_1) - \frac{m_{\mathrm{t}}}{m}\frac{\omega}{m_{\mathrm{t}}} f_2(\gamma_1) - \left(\frac{1}{4}\frac{m_{\mathrm{t}}^2}{m^2} + \left(1+\frac{\omega^2}{m_{\mathrm{t}}^2}\right)\Delta^{\mathrm{T,L}}\right) f_1(\gamma_1)\right], \tag{11}$$

where the weight factors f_k read

$$f_k(\gamma_1) := \int_{\gamma_1}^{\infty} \frac{\gamma^{k-2}\,\mathrm{d}\rho_{\mathrm{F}}(\gamma)}{\sqrt{\gamma^2-1}}, \tag{12}$$

with density $\mathrm{d}\rho_{\mathrm{F}}(\gamma)$ in (5).

The quasiclassical fugacity expansion of the spectral functions (11) is found by expanding density (5) in ascending powers of $\mathrm{e}^{-\hat{\alpha}}$. In leading order, $\mathrm{d}\rho_{\mathrm{F}}(\gamma) \sim \mathrm{d}\rho_{\alpha,\beta}(\gamma)$,

$$\mathrm{d}\rho_{\alpha,\beta}(\gamma) = A_{\alpha,\beta}\gamma^{-\alpha-1}\mathrm{e}^{-\beta\gamma}\sqrt{\gamma^2-1}\,\mathrm{d}\gamma, \quad A_{\alpha,\beta} := \frac{m^3 V}{\pi^2}\mathrm{e}^{-\hat{\alpha}}. \tag{13}$$

This power-law density is the classical limit of the fermionic density $\mathrm{d}\rho_{\mathrm{F}}$. As mentioned above, exponent $\hat{\alpha}$ in the normalization factor $A_{\alpha,\beta}$ defines the fugacity, and is not to be confused with the electron index $\alpha = \delta - 2$ in (13). The leading order of the reduced spectral functions (12) can be written as incomplete Γ-function, $f_k(\gamma_1) \sim A_{\alpha,\beta}\beta^{\delta-k}\Gamma(k-\delta,\beta\gamma_1)$, obtained by replacing the fermionic $\mathrm{d}\rho_{\mathrm{F}}$ in the weights (12) by the Boltzmann power-law density (13).

The classical limit of the fermionic spectral functions $F^{\mathrm{T,L}}(\omega,\gamma_1)$ in (8) is the Boltzmann average [31]

$$B^{\mathrm{T,L}}(\omega,\gamma_1) := \int_{\gamma_1}^{\infty} p_{\mathrm{cl}}^{\mathrm{T,L}}(\omega,\gamma)\,\mathrm{d}\rho_{\alpha,\beta}(\gamma). \tag{14}$$

Here, $p_{\mathrm{cl}}^{\mathrm{T,L}}(\omega,\gamma)$ is the classical tachyonic spectral density, recovered by dropping all terms containing m_{t}/m ratios in (3) and (4). In particular, $\Delta_{\mathrm{cl}}^{\mathrm{T}} = 1$ and $\Delta_{\mathrm{cl}}^{\mathrm{L}} = 0$, cf. (3). The classical spectral functions $B^{\mathrm{T,L}}(\omega,\gamma_1)$ are obtained from the Fermi functions $F^{\mathrm{T,L}}(\omega,\gamma_1)$ in (11) by dropping the m_{t}/m terms, and substituting the leading order of the fugacity expansion of the weights $f_k(\gamma_1)$ as stated after (13). The classical limit of the fermionic spectral average $\langle p^{\mathrm{T,L}}(\omega)\rangle_{\mathrm{F}}$ in (10) thus reads

$$\left\langle p^{\mathrm{T,L}}(\omega)\right\rangle_{\alpha,\beta} = B^{\mathrm{T,L}}(\omega,\gamma_1)\theta(\omega_{1,\mathrm{cl}}-\omega) + B^{\mathrm{T,L}}\Big(\omega,\sqrt{1+\omega^2/m_{\mathrm{t}}^2}\Big)\theta(\omega-\omega_{1,\mathrm{cl}}), \tag{15}$$

where $\omega_{1,\mathrm{cl}} := m_{\mathrm{t}}\sqrt{\gamma_1^2-1}$ is the classical limit of the break frequency (9).

3. Spectral curvature of Galactic and extragalactic TeV γ-ray sources: Does distance matter?

The spectral fits of the active galactic nuclei (AGNs) and the Galactic TeV sources in Figs. 1–4 are based on the E^2-rescaled flux densities

$$E^2\frac{\mathrm{d}N^{\mathrm{T,L}}}{\mathrm{d}E} = \frac{\omega}{4\pi d^2}\left\langle p^{\mathrm{T,L}}(\omega)\right\rangle_{\alpha,\beta}, \tag{16}$$

where d is the distance to the source and $\langle p^{\mathrm{T,L}}(\omega)\rangle_{\alpha,\beta}$ the spectral average (15) (with $\omega = E/\hbar$). The fits are done with the unpolarized flux density $\mathrm{d}N^{\mathrm{T+L}} = \mathrm{d}N^{\mathrm{T}} + \mathrm{d}N^{\mathrm{L}}$ of two electron populations $\rho_{i=1,2}$, cf. Table 1. Each electron density generates a cascade ρ_i, and the wideband comprises two cascade spectra labeled ρ_1 and ρ_2 in the figures. As for the electron count, $n_1 := \int_{\gamma_1}^{\infty}\mathrm{d}\rho_{\alpha,\beta}(\gamma)$, we use a rescaled parameter $\hat{n}_1$ for the fit,

$$\hat{n}_1 := \frac{\alpha_{\mathrm{q}} n_1}{\hbar[\mathrm{keV\,s}]4\pi d^2[\mathrm{cm}]} \approx 1.27 \times 10^{-45}\frac{n_1}{d^2[\mathrm{Mpc}]}, \tag{17}$$

which is independent of the distance estimate in (16). Here, $\hbar[\mathrm{keV\,s}]$ implies the tachyon mass in keV units, that is, we put $m_{\mathrm{t}} \approx 2.15$ in the spectral densities (3). At γ-ray energies, only a tiny $\alpha_{\mathrm{q}}/\alpha_{\mathrm{e}}$-fraction (the ratio of tachyonic and electric fine structure constants) of the tachyon flux is absorbed by the detector, which requires a rescaling of the electron count n_1, so that the actual number of radiating electrons is $n_1^{\mathrm{e}} = n_1\alpha_{\mathrm{e}}/\alpha_{\mathrm{q}} \approx 7.3 \times 10^{10} n_1$, cf. Ref. [12]. We thus find the electron count as $n_1^{\mathrm{e}} \approx 5.75 \times 10^{55}\hat{n}_1 d^2[\mathrm{Mpc}]$, where $\hat{n}_1$ defines the tachyonic flux amplitude extracted from the spectral fit. (In Table 1, the subscript 1 of $\hat{n}_1$ and n_1^{e} has been dropped.) Electron temperature and cutoff parameter in the Boltzmann factor of density (13) are related by $kT[\mathrm{TeV}] \approx 5.11 \times 10^{-7}/\beta$, and the energy estimates of the thermal cascades in Table 1 are based on $U[\mathrm{erg}] \sim 2.46 \times 10^{-6} n_1^{\mathrm{e}}/\beta$, cf. Ref. [18]. (The renormalized count $n_1^{\rm e}$ is to be identified with the particle number N in the thermodynamic functions discussed in this reference.) The distance estimates of the AGNs are based on $d \sim cz/H_0$, with the Hubble distance $c/H_0 \approx 4.4 \times 10^3$ Mpc (that is, $h_0 \approx 0.68$). Hence, $d[\text{Mpc}] \approx 4.4 \times 10^3 z$, and $n_1^{\rm e} \approx 1.1 \times 10^{63} \hat{n}_1 z^2$, cf. Table 1.

Fig. 1 shows the tachyonic spectral map of the BL Lacertae object (BL Lac) 1ES 0229+200, located at a redshift of $z \approx 0.140$, cf. Refs. [1–4]. The flux points were obtained with the HESS array of atmospheric Cherenkov telescopes in the Khomas Highland of Namibia [4]. The χ^2-fit is done with the unpolarized tachyon flux T + L, and subsequently split into transversal and longitudinal components. The differential flux is rescaled with E^2 for better visibility of the spectral curvature. Temperature and source count of the electron populations generating the cascades are recorded in Table 1. In Fig. 2, we show the spectral map of the BL Lac 1ES 0347-121, at a redshift of $z \approx 0.188$, cf. Refs. [5–7]. TeV γ-ray spectra of BL Lacs are usually assumed to be generated by inverse Compton scattering or proton–proton scattering followed by pion decay [8]. Both mechanisms result in a flux of TeV photons, assumed to be partially absorbed by interaction with infrared background photons owing to pair creation, so that the intrinsic spectrum has to be reconstructed on the basis of intergalactic absorption models depending on vaguely known cosmological input parameters [9]. The extragalactic tachyon flux is not attenuated by interaction with the background light, there is no absorption of tachyonic γ-rays. The superluminal Proca field (1) is minimally coupled to the electron current, and does not directly interact with electromagnetic radiation.

The spectral curvature apparent in double-logarithmic plots of the E^2-rescaled flux densities (16) is intrinsic, caused by the Boltzmann factor of the electron populations generating the tachyon flux. The curvature present in TeV γ-ray spectra does not increase with distance, at least there is no evidence to that effect if we compare the spectral slopes of the blazars in Figs. 1 and 2, and the spectral maps of other flaring AGNs such as H1426+428 at $z \approx 0.129$ and 1ES 1959+650 at $z \approx 0.047$, cf. Ref. [11]. Further evidence for intrinsic spectral curvature is provided by Fig. 3, depicting the spectral map of the microquasar LS 5039, a compact object orbiting a massive O-star [32–34]. The spectral curvature of this Galactic binary is even more pronounced than of the BL Lacs in Figs. 1 and 2. The same holds true for the HESS spectral map of LS 5039 at the inferior conjunction studied in Ref. [18].

Fig. 4 depicts the γ-ray wideband of the TeV source HESS J1801-233 and the coincident EGRET point source 3EG J1800-2338 [35–37]. The extended TeV source is located on the northeastern rim of the supernova remnant (SNR) W28, a mixed-morphology SNR interacting with molecular clouds [38,39]. The spectral map of SNR W28 in Fig. 4 is to be compared to the unpulsed γ-ray spectrum of the Crab Nebula, cf. Fig. 1 in Ref. [11], the spectral map of SNR RX J1713.7-3946 in Fig. 2 of Ref. [11], and in particular to the unidentified TeV source TeV J2032+4130 in conjunction with the associated EGRET source 3EG J2033+4118, cf. Fig. 6 of Ref. [12]. A spectral plateau in the MeV to GeV range occurs frequently in spectral maps of TeV γ-ray sources, and can easily be fitted with tachyonic cascade spectra, in contrast to electromagnetic inverse-Compton fits. SNR W28 is located at a distance of 1.9 kpc [38]. The thermal cascade in the MeV range (ρ_2 in Fig. 4) preceding the spectral plateau is strongly curved; the power-law slope of the ρ_1 cascade also terminates in exponential decay, but outside the presently accessible TeV range shown in the figure. The cutoff temperature of the nonthermal electron density generating cascade ρ_1 is too high to bend the power-law slope in the TeV range covered in Fig. 4, so that the internal energy of the shock-heated plasma could not be determined from the χ^2-fit, in contrast with the power-law index α and the threshold Lorentz factor γ_1, cf. caption to Table 1.

4. Conclusion

The spectral maps of two TeV γ-ray blazars have been fitted with tachyonic cascade spectra and compared to a Galactic γ-ray binary and supernova remnant. Table 1 contains estimates of the thermodynamic parameters of the electron populations generating the superluminal cascades. The spectral curvature is intrinsic and reproduced by the tachyonic spectral densities (3) averaged with ultra-relativistic thermal electron distributions, cf. Figs. 1–3. The shocked electron plasma in SNR W28 requires a nonthermal power-law distribution to adequately reproduce the TeV cascade in Fig. 4. The curvature in the γ-ray spectra of BL Lacs is uncorrelated with distance, so that absorption of electromagnetic radiation due to interaction with infrared photons is not an attractive explanation of spectral curvature. By contrast, there is no attenuation of the extragalactic tachyon flux, as tachyons cannot interact with cosmic background photons, so that the observed cascades are the intrinsic spectrum. The distance of the AGNs does not show in the spectral curvature, as tachyonic cascades are unaffected by background photons.

Acknowledgements

The author acknowledges the support of the Japan Society for the Promotion of Science. The hospitality and stimulating atmosphere of the Centre for Nonlinear Dynamics, Bharathidasan University, Trichy, and the Institute of Mathematical Sciences, Chennai, are likewise gratefully acknowledged.

References

[1] R. Falomo, J.K. Kotilainen, Astron. Astrophys. 352 (1999) 85.
[2] D. Horan, et al., Astrophys. J. 603 (2004) 51.
[3] D.A. Williams, AIP Conf. Proc. 745 (2005) 499.
[4] F. Aharonian, et al., Astron. Astrophys. 475 (2007) L9.
[5] C.M. Urry, et al., Astrophys. J. 532 (2000) 816.
[6] M. Giroletti, et al., Astrophys. J. 613 (2004) 752.
[7] F. Aharonian, et al., Astron. Astrophys. 473 (2007) L25.
[8] K. Tsuchiya, et al., Astrophys. J. 606 (2004) L115.
[9] J. Albert, et al., Astrophys. J. 662 (2007) 892.
[10] R. Tomaschitz, Eur. Phys. J. D 32 (2005) 241.
[11] R. Tomaschitz, Eur. Phys. J. C 49 (2007) 815.
[12] R. Tomaschitz, Ann. Phys. 322 (2007) 677.
[13] S. Tanaka, Prog. Theor. Phys. 24 (1960) 171.
[14] Ya.P. Terletsky, Sov. Phys. Dokl. 5 (1961) 782.
[15] R. Tomaschitz, Class. Quantum Grav. 18 (2001) 4395.
[16] R. Tomaschitz, Eur. Phys. J. B 17 (2000) 523.
[17] W.-M. Yao, et al., J. Phys. G 33 (2006) 1.
[18] R. Tomaschitz, Physica A 385 (2007) 558.
[19] R. Tomaschitz, Physica A 387 (2008) 3480.
[20] S.P. Reynolds, J.W. Keohane, Astrophys. J. 525 (1999) 368.
[21] R. Enomoto, et al., Astrophys. J. 652 (2006) 1268.
[22] T. Nakamori, et al., Astrophys. J. 677 (2008) 297.
[23] J.M. Fierro, et al., Astrophys. J. 494 (1998) 734.
[24] R. Tomaschitz, Astropart. Phys. 23 (2005) 117.
[25] R. Tomaschitz, Astropart. Phys. 27 (2007) 92.
[26] R. Tomaschitz, Physica A 335 (2004) 577.
[27] I. de Pater, B.J. Butler, Icarus 163 (2003) 428.
[28] I. de Pater, et al., Icarus 163 (2003) 434.
[29] R. Tomaschitz, Physica A 320 (2003) 329.
[30] R. Tomaschitz, Eur. Phys. J. C 45 (2006) 493.
[31] R. Tomaschitz, Phys. Lett. A 366 (2007) 289.
[32] F. Aharonian, et al., Astron. Astrophys. 460 (2006) 743.
[33] M.V. McSwain, et al., Astrophys. J. 600 (2004) 927.
[34] J. Casares, et al., Mon. Not. R. Astron. Soc. 364 (2005) 899.
[35] F. Aharonian, et al., Astron. Astrophys. 481 (2008) 401.
[36] R.C. Hartman, et al., Astrophys. J. Suppl. 123 (1999) 79.
[37] L. Zhang, K.S. Cheng, Astron. Astrophys. 335 (1998) 234.
[38] P.F. Velázquez, et al., Astron. J. 124 (2002) 2145.
[39] J. Rho, K.J. Borkowski, Astrophys. J. 575 (2002) 201.